

Physically-based Lighting Augmentation for Robotic Manipulation

Shutong Jin^{1*}, Lezhong Wang^{2*}, Ben Temming¹, Florian T. Pokorny¹

¹KTH Royal Institute of Technology, ²Technical University of Denmark

*Equal Contribution

{shutong, temming, fpokorny}@kth.se, lewa@dtu.dk

Abstract: Despite advances in data augmentation, policies trained via imitation learning still struggle to generalize across environmental variations such as lighting changes. To address this, we propose the first framework that leverages physically-based inverse rendering for lighting augmentation on real-world human demonstrations. Specifically, inverse rendering decomposes the first frame in each demonstration into geometric (surface normal, depth) and material (albedo, roughness, metallic) properties, which are then used to render appearance changes under different lighting. To ensure consistent augmentation across each demonstration, we fine-tune Stable Video Diffusion on robot execution videos for temporal lighting propagation. We evaluate our framework by measuring the structural and temporal consistency of the augmented sequences, and by assessing its effectiveness in reducing the behavior cloning generalization gap (40.1%) on a 7-DoF robot across 6 lighting conditions using 720 real-world evaluations. We further showcase three downstream applications enabled by the proposed framework.

Keywords: Robotic Manipulation, Lighting Augmentation, Imitation Learning

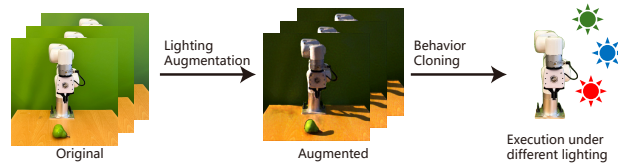


Figure 1: Our framework enables relighting of real-world human demonstrations through inverse rendering, improving imitation learning performance under diverse lighting conditions.

1 Introduction

Imitation learning offers a promising approach to deploying various robotic manipulation tasks using expert human demonstrations [1, 2, 3]. However, as pointed out by previous research [4, 5, 6, 7, 8, 9, 10, 11, 12, 13], a critical challenge remains: the trained policies often *struggle to generalize across variations in lighting, object texture and visual distractors*. Capturing variations in these individual factors in real-world datasets is resource-intensive, and this challenge is further compounded when considering their combinations, making it difficult to address with real-world data collection alone.

Image augmentation techniques are widely adopted to improve generalization across environmental variations without requiring additional data collection. For example, domain randomization [14, 15] typically alters environmental parameters like backgrounds in simulation or applies visual perturbations like color jitter. Generative models have also been used to augment object textures and add visual distractors [4, 16, 17]. However, explicit modeling and manipulation of lighting in real-world demonstrations remains underexplored, largely due to the difficulty of recovering geometric and material information required for simulating accurate light–material interactions.

In this paper, we propose the **first framework that applies physically-based inverse rendering for geometry- and material-aware lighting augmentation for imitation learning from real-world demonstrations in robotic manipulation**. Our contributions are fourfold:

- **Modular Integration.** We adopt an inverse rendering module [18] to decompose a single demonstration frame into geometric and material properties, which are then used by a rendering module to simulate new lighting on the decomposed properties.
- **Domain-Adapted Stable Video Diffusion.** To ensure consistent augmentation across consecutive frames of each demonstration, we fine-tune Stable Video Diffusion (SVD) [19] for temporal lighting propagation. Fine-tuning data includes synthetic robot execution videos from Factor World [5] with varied lighting across tasks, and real-world execution videos from RoboNet [20] with visual degradation for radiometric accuracy.
- **Real-world Evaluation.** We validate our framework by assessing structural and temporal consistency in augmented demonstrations, and through **real-world experiments** on a 7-DoF robot with an embodiment unseen during SVD fine-tuning. Under six varied lighting conditions, our method reduces the behavior cloning generalization gap by 40.1% across **720 evaluations on two tasks**, compared to models trained without lighting augmentation.
- **Downstream Applications.** We showcase augmentations on three additional environmental factors using geometric and material properties estimated by our framework.

2 Related Work

Data Augmentation for Robotic Manipulation. Domain randomization [21, 22, 23, 24] has been widely studied to enhance policy robustness when transferring from simulation to the real world. Building upon this, recent efforts [4, 17, 16, 25, 26] have focused on semantic augmentation of real-world images leveraging text-driven generative models [27, 28] to introduce texture variation, visual distractors, etc. For example, ROSIE [17] proposes changing object textures by first segmenting augmentation regions [29] and then performing text-guided image inpainting [30]. Rendering techniques [31, 32, 33] have also been applied for viewpoint augmentation [34, 35, 36, 37]. Another line of work breaks long-horizon tasks into object-centric subtasks or manipulation skills and replays transformed demonstrations in simulation to generate new data from a limited number of examples [38, 39, 40, 41, 42]. In this paper, we focus on the underexplored problem of lighting augmentation on real-world human demonstrations for robotic manipulation.

Inverse Rendering and Relighting. Relighting a scene typically requires identifying and altering its properties to produce the intended lighting effect [43]. Inverse rendering facilitates this by providing separate or joint estimations of geometry [44, 45, 46], material [47, 48, 49], and lighting [50, 51, 52] in a scene. Based on input requirements, inverse rendering can be categorized into single-view [53, 54, 55] and multi-view [56, 57, 58] methods. While methods such as DPI [59] and FIPT [60] produce high-fidelity relighting results, they rely on multi-view inputs for scene reconstruction and domain-specific datasets [61], making them incompatible with most existing robotic dataset camera setups. In this work, **we present the first integration of single-view inverse rendering into robotic manipulation for explicit modeling of scene geometry and material properties.**

3 Approach

3.1 Formulation and Overview

Given one episode of real-world human demonstration ($\mathbf{I}, \mathbf{P}, \mathbf{A}$) recorded from a fixed viewpoint, where $\mathbf{I} \in \mathbb{R}^{H \times W \times 3 \times T}$ represents a sequence of T RGB images, $\mathbf{P} \in \mathbb{R}^{p \times T}$ denotes proprioception states, and $\mathbf{A} \in \mathbb{R}^{a \times T}$ corresponds to actions, our goal is to perform physically-based lighting augmentation on \mathbf{I} to produce a relit sequence \mathbf{I}^* from the same viewpoint, while preserving struc-

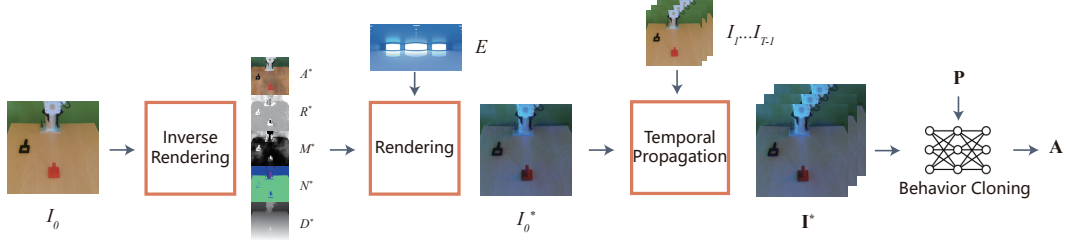


Figure 2: Given the first frame I_0 in a real-world human demonstration, the inverse rendering module estimates material (A^* , R^* , M^*) and geometric (N^* , D^*) properties. The rendering module uses these estimates and an environment map E providing new lighting to produce a relit frame I_0^* . The new lighting is then propagated across the entire sequence \mathbf{I} , producing \mathbf{I}^* and forming an augmented episode (\mathbf{I}^* , \mathbf{P} , \mathbf{A}) for behavior cloning.

tural and temporal consistency. Here, *physically-based* refers to physically-based rendering (PBR) for accurate light-material interactions.

Overview. As shown in *Fig. 2* the proposed framework consists of three components: (1) we begin by selecting the first frame I_0 from \mathbf{I} and applying inverse rendering (*Sec. 3.2*) to estimate the geometric and material properties of the scene depicted in I_0 ; (2) the rendering module (*Sec. 3.3*) then uses the estimated properties and an environment map E to relight I_0 , producing I_0^* ; and (3) the temporal propagation module (*Sec. 3.4*) propagates the lighting from I_0^* across the full image sequence \mathbf{I} , resulting in the final augmented sequence \mathbf{I}^* . This forms an augmented episode (\mathbf{I}^* , \mathbf{P} , \mathbf{A}), which is then used to train the behavior cloning policy. The environment map E has two use cases: (1) approximating the current lighting conditions to train a policy adapted to the environment (*Sec. 4.2*), and (2) introducing diverse lighting to contribute to a lighting-invariant policy (*Sec. 5*).

3.2 Single-Frame Inverse Rendering

Following [18], we use a pre-trained network \mathcal{P} to predict geometric and material properties of the scene depicted in I_0 :

$$A_p, R_p, M_p, N_p, D_p = \mathcal{P}(I_0), \quad (1)$$

where A_p , R_p , and M_p are predicted material properties (albedo, roughness, metallic), and N_p and D_p are predicted geometric properties (surface normal and depth). Examples of predicted properties can be found in *Fig. 2*. All predictions share the spatial resolution of I_0 . Final property estimates are derived by minimizing the following objective:

$$A^*, R^*, M^*, N^*, D^* = \arg \min_{A_p, R_p, M_p, N_p, D_p} \mathcal{L}_p(I_0, I_p), \quad (2)$$

where I_p denotes the frame rendered using the predicted properties. $\mathcal{L}_p = \mathcal{L}_{re} + \delta \mathcal{L}_{cons}$, where \mathcal{L}_{re} denotes the reconstruction loss between the rendered frame I_p and the original frame I_0 , and \mathcal{L}_{cons} enforces consistency between the optimized and originally predicted properties, scaled by a factor δ . Further details are provided in the supplementary material.

3.3 Single-Frame Relighting

To perform physically-based relighting, we render new lighting based on incoming radiance directions and modeled scene properties.

Light Sampling. Given an environment map $E \in \mathbb{R}^3$, the incoming radiance λ in direction ω_i is sampled as:

$$\lambda(\omega_i) = E(\omega_i), \quad (3)$$

where E is obtained either by approximating [18] or measuring [62, 63] the current lighting condition using graphics techniques, or by selecting from open-source HDRI datasets [64, 65].

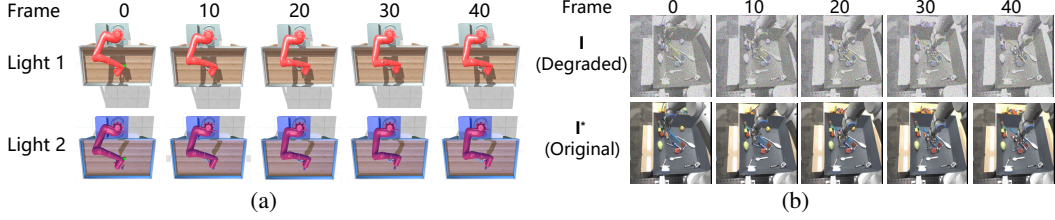


Figure 3: (a) Examples of synthetic robot execution videos with lighting variations. (b) Examples of real-world robot execution videos with visual degradation.

Scene Modeling. The estimated properties from *Sec. 3.2* are used to model the material appearance \mathcal{M} along direction ω_i of the scene depicted in I_0 , using the widely adopted Disney BRDF [66]:

$$\mathcal{M}(\omega_i) = (1 - M^*)f_{diffuse}(A^*, R^*, N^*) + f_{specular}(R^*, N^*), \quad (4)$$

where $f_{diffuse}$ and $f_{specular}$ model the diffuse and specular components of reflection, respectively; further details are provided in the supplementary material.

Scene Relighting. Using the simplified rendering equation [67], the augmented frame I_0^* under new lighting from environment map E is computed as:

$$I_0^* = \int_{\Omega} \mathcal{M}(\omega_i)\lambda(\omega_i)(\omega_i \cdot N^*) d\omega_i, \quad (5)$$

where Ω is the hemisphere centered at surface normal N^* , containing all incoming directions ω_i . Note that once the property estimation for I_0 from *Sec. 3.2* is completed, multiple augmentations can be applied using the same set of estimated properties.

3.4 Temporal Propagation

Domain-Adapted Stable Video Diffusion. To meet the temporal consistency requirements of robotic manipulation, we adopt Stable Video Diffusion (SVD) [19] for its temporal modeling capabilities to propagate lighting from I_0^* across the entire demonstration. We formulate this as a video-to-video translation task: lighting from the original image sequence \mathbf{I} is transferred to generate the augmented sequence \mathbf{I}^* , guided by the reference frame I_0^* . This is defined as:

$$\mathbf{I}^* = \delta(I_0^*, \mathbf{I}_{input}), \quad \mathbf{I}_{input} = \text{Concatenate}(I_0^*, \mathbf{I}_{1:T-1}), \quad (6)$$

where δ denotes the SVD model.

Robotic Relighting Data Curation. It’s important to note that the vanilla SVD underperforms in this task due to the absence of robotic elements like arms and grippers in its training data, resulting in a severely cartoonish appearance in generated robotic scenes. Following SVD’s original fine-tuning paradigm, we construct two datasets for different stages of fine-tuning:

- Synthetic videos with lighting variation (\mathcal{D}_1 , *Fig. 3a*). We generate domain-specific relighting data for robotic manipulation using the Factor World [5] benchmark, introducing lighting variation under identical task execution trajectories. All 42 built-in scenes covering 19 tasks (e.g., door opening) are used, each captured with six camera views: one fixed top-down and five randomized within constrained azimuth, inclination, and radius in the range $[-\pi/2, \pi/2]$ to ensure robot visibility. Each scene includes 30 lighting conditions by sampling ambient and diffuse RGB values from $[25, 255]$. Videos are rendered at 512×512 resolution with 100 frames at 24 fps. For fine-tuning, we randomly select pairs of videos showing the same task trajectories under different lighting, using one as the input \mathbf{I} and the other as the target sequence \mathbf{I}^* .
- Real-world videos with visual degradation (\mathcal{D}_2 , *Fig. 3b*). Since existing real-world robotic datasets lack perfectly paired original and relit videos under identical task execution trajectories, we manually create video pairs by applying visual degradation on original videos

from RoboNet [20] with 15 million video frames from 7 different robot platforms. We apply random visual transformations by sampling brightness, contrast, and saturation scaling factors from $[0.2, 1.9]$, and hue shifts from $[-0.5, 0.5]$. The degraded robot execution video serves as the input \mathbf{I} , while the original video acts as the output \mathbf{I}^* .

Fine-tuning. We fine-tune SVD in two stages. In Stage 1, we use synthetic videos from \mathcal{D}_1 , which provide the main data for domain adaptation and reduce overfitting via controlled lighting variation. However, due to the non-physically-based lighting in Factor World, this stage lacks radiometric accuracy, motivating fine-tuning on real-world videos from \mathcal{D}_2 in Stage 2. Fine-tuning is performed on a pretrained 14-frame SVD model using a single H100 GPU for 8,000 steps for Stage 1 and 1,000 steps for Stage 2. A limited number of steps are applied to Stage 2 due to the absence of ground-truth relit pairs. Further details and ablation studies are provided in the supplementary material.

4 Experiments

4.1 Visual Lighting Quality Evaluation

We apply lighting augmentation to 10 randomly selected sequences (600 frames) from the real-world human demonstrations in Sec.4.2 using our method and IC-Light [68], a widely recognized text-prompt-based relighting method. Ground-truth episodes are recorded under a side-mounted blue LED panel light under the same task execution trajectories. Two sets of metrics are adopted: (1) *LPIPS* [69] and *SSIM* [70] are computed between the ground-truth and relit image sequences to assess structural consistency and fidelity. (2) *Temporal LPIPS* and *Temporal SSIM* are computed between consecutive frames in the relit sequences to assess temporal consistency. Since IC-Light does not support video relighting, we apply it frame-by-frame using a fixed random seed and the prompt “blue LED light” for consistency. We perform relighting using an environment map approximated from the ground truth episodes with [18]. Qualitative and quantitative evaluation results can be found in Fig. 4. Our method achieves better performance by estimating scene-level properties, which are more compatible with robotic settings, whereas IC-Light’s foreground/background separation is better suited for human relighting. Our temporal propagation module further improves visual consistency by reducing abrupt changes between frames.

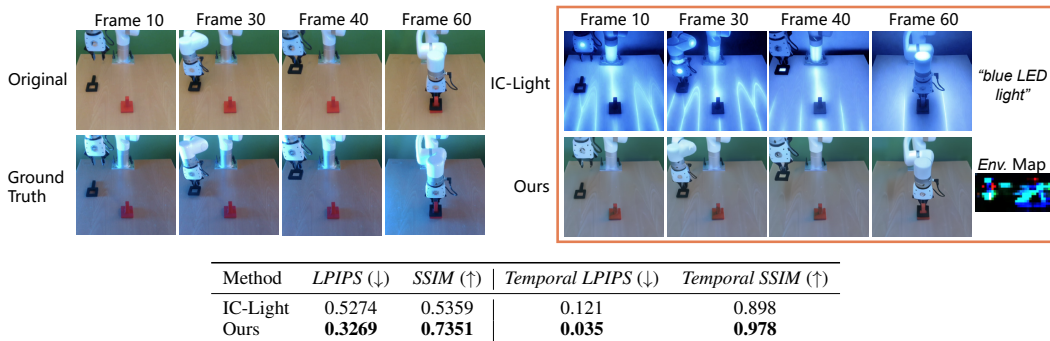


Figure 4: Qualitative (top) and quantitative (bottom) evaluation of lighting augmentation. Although exceeding the baseline, the lighting in our augmented episodes appears more diffused compared to the ground truth, as indicated by weaker side shadows. This discrepancy mainly results from the rough environment map approximation (32×16 resolution) without specialized graphics equipment.

4.2 Real-world Evaluation

Lighting Setup. White light with minimal shadows (*Ambient*, Fig. 5a) is used during expert human demonstration collection for policy training. During evaluation, six lighting conditions are designed using a programmable RGB LED panel. This includes two sets with different evaluation purposes: (1) Daily-use conditions — *Side* (strong shadows), *Regional* (blue regional highlight), and *Dim*

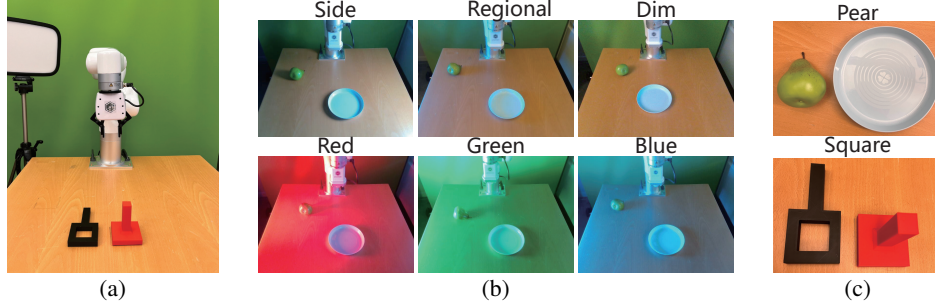


Figure 5: (a) Experimental setup under *Ambient* lighting. (b) The six lighting conditions used for generalization gap evaluation. (c) Objects used in the two manipulation tasks.

(low-light); (2) Artificial RGB lighting — *Red*, *Green*, and *Blue* — with illuminance levels of 4,600 lux and RGB values (255, 0, 0), (0, 255, 0), and (0, 0, 255), respectively, designed to evaluate each policy under single-source lighting. These colors are chosen based on the principle of light transport linearity, which allows any colored illumination to be reconstructed as their linear combination. Examples are shown in *Fig. 5b*.

Manipulation Tasks. *Pear*: Grasp a randomly placed green plastic pear using a vacuum gripper and place it on a plate. *Square*: Grasp a randomly placed black square nut by its handle using a parallel jaw gripper and insert it into a matching red square peg. To better assess performance under challenging lighting conditions, we report performance separately for the reaching (*R*) subtask, which involves reaching the area of the pear or square nut, and the pick-and-place (*PnP*) outcome, defined as successfully picking up the object and placing it in the corresponding plate or peg.

Implementation Details. We perform behavior cloning using ResNet18 [71] and Multi-Layer Perceptron (BC-MLP) to map features to actions. Random cropping (*Crop*) is used as the default augmentation due to its widespread use and proven effectiveness [5, 39]. We evaluate two variants: *+Jitter*, which adds color jitter, and *+Ours*, which adds our proposed lighting augmentation. Color jitter is selected as a baseline due to its ability to mitigate the impact of color and illumination variation. Training and evaluation are conducted on a 7-DoF UFactory XArm7 robot observed by a single externally mounted RGB camera. Each task uses 200 human demonstrations to train the baseline policies *Crop* and *+Jitter*. For *+Ours*, 10 demonstrations are randomly selected and augmented with six environment maps approximating the six evaluation lighting conditions, producing 260 training episodes per task for policy training. See the supplementary material for full implementation details.

Evaluation Protocol. For each combination of task τ , lighting condition L , and augmentation method Aug , we conduct 20 real-world evaluations. The success rate for each combination is denoted as $S_L^{Aug}(\tau)$. We use BC-MLP trained and evaluated under *Ambient* lighting with *Crop* augmentation as the base policy. The corresponding subtask success rates are: $S_{Ambient}^{Crop}(Pear-R) = 1.00$, $S_{Ambient}^{Crop}(Pear-PnP) = 0.60$, $S_{Ambient}^{Crop}(Square-R) = 1.00$, $S_{Ambient}^{Crop}(Square-PnP) = 0.85$. Performance degradation under unseen evaluation lighting conditions is measured by the *Generalization Gap*, defined as the normalized drop in success rate relative to the base policy:

$$Generalization\ Gap = (S_{Ambient}^{Crop}(\tau) - S_L^{Aug}(\tau)) / S_{Ambient}^{Crop}(\tau). \quad (7)$$

Results. *Tab. 1* presents the generalization gap of BC-MLP under six unseen lighting conditions across 720 real-world evaluations. Averaged over both subtasks across the two tasks, our method outperforms *Crop* by 40.1% and *+Jitter* by 35.7%. In the daily-use lighting set, *Crop* shows a major drop in performance, except under *Dim*. While *+Jitter* performs reasonably on the reaching subtask, it consistently fails in the final pick-and-place outcome. *+Ours* improves performance across both subtasks under these conditions. In the artificial RGB lighting set, both *Crop* and *+Jitter* fail in most cases, even on the reaching subtask. Interestingly, *+Jitter* displays strong preferences for

Table 1: Generalization Gap (\downarrow) with different augmentation methods under unseen lighting. The best-performing policy is in bold, and the second-best is underscored.

Lighting	Crop				+Jitter				+Ours			
	Pear		Square		Pear		Square		Pear		Square	
	R	PnP	R	PnP	R	PnP	R	PnP	R	PnP	R	PnP
Side	1.00	1.00	1.00	1.00	0.70	1.00	0.85	1.00	<u>0.92</u>	1.00	0.10	0.53
Regional	0.95	1.00	1.00	1.00	<u>0.55</u>	1.00	<u>0.50</u>	1.00	0	0.67	0	0.47
Dim	0	0.16	<u>0.05</u>	0.35	0.1	0.83	<u>0.05</u>	0.47	0	<u>0.34</u>	0	0.06
Red	1.00	1.00	1.00	1.00	<u>0.70</u>	1.00	<u>0.90</u>	1.00	0.40	1.00	0.10	1.00
Green	<u>0.85</u>	1.00	<u>0.90</u>	1.00	1.00	1.00	0.95	1.00	0	1.00	0	0.88
Blue	1.00	1.00	0.95	1.00	1.00	1.00	<u>0.55</u>	1.00	0.15	0.92	0.05	1.00

different RGB lighting in the two tasks, likely due to its use of global color shifts. Our method maintains strong reaching performance but struggles with pick-and-place in these more extreme lighting conditions. Common failure modes for *Crop* and *+Jitter* involve moving directly to the plate or peg without interacting with the pear or nut. Failures in *+Ours* often involve reaching the pear or nut with the gripper open and hovering just above the object, without executing a pick action. This may relate to the altered object appearance under high-intensity lighting (4,600 lux), where high reflectivity could disrupt perception. See the limitations section for further details and the supplementary video for examples of common failure modes across different methods.

4.3 Ablation Study

Impact of the Number of Lighting Conditions for Augmentation.

We perform augmentation using 1 (*Red*), 3 (*Red*, *Green*, *Blue*), 6 (all conditions from *Sec. 4.2*), and 9 lighting conditions (6 plus three additional lights with RGB values (255, 255, 0), (255, 0, 255), and (0, 255, 255)). Evaluation is performed in single-source *Red* light to control for lighting composition effects and isolate augmentation impact. Reaching success rates on *Square* task, averaged over 10 trials, are shown in *Fig. 6a*. Including the currently observed lighting (*Red*) in augmentation immediately boosts performance (from 0%). However, performance degrades when too many unrelated lighting conditions are added, likely due to the reduced presence of target augmentations (*Red*) in the expanded set. See *Sec. 7* for further discussion.

Impact of the Number of Episodes for Augmentation. We select 10, 25, 75, and 100 episodes from 200 demonstrations and augment each with six lighting conditions. Evaluation follows the same setup as above. As shown in *Fig. 6b*, performance is relatively unaffected by the number of augmented episodes, with no signs of overfitting — possibly due to the lighting diversity within each episode. To save computation, we use the minimal setting of 10 episodes for augmentation.

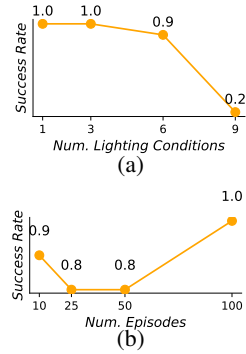


Figure 6: Ablation study: (a) effect of the number of lighting conditions; (b) effect of the number of augmented episodes.

5 Applications

Through scene decomposition via inverse rendering, we extend our framework to augment three additional environmental factors (background, object texture, and distractors) beyond lighting (*Fig. 7a*) on existing datasets, as demonstrated on BridgeData v2 [72].

5.1 Background Augmentation

Background appearance is tied to global illumination; therefore, we render segmented scene geometry with different environment maps to create new backgrounds with corresponding lighting. Scene geometry is reconstructed by triangulating the depth map D^* from *Sec. 3.2* into a mesh Λ :

$$\Lambda = \text{Triangulate} (K^{-1}[x \ y \ 1]^T D^*(x, y)), \quad (8)$$

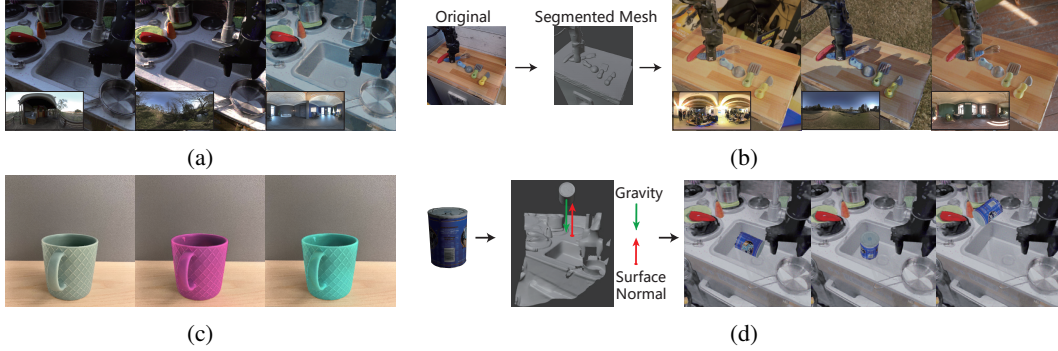


Figure 7: Examples of applications: (a) Lighting augmentation with different environment maps; (b) Background augmentation with different environment maps; (c) Texture augmentation via albedo adjustment; (d) Gravity-based distractor placement, with distractor mesh sourced from [74].

where K is a fixed intrinsic matrix of a pinhole camera, and $D^*(x, y)$ is the depth at pixel (x, y) . We then project 2D segmentation masks [73] onto the mesh Λ from the default viewpoint to isolate and segment the robot arm and task area. The segmented mesh is then rendered with various environment maps to produce new backgrounds and lighting. Examples are shown in Fig. 7b.

5.2 Object Texture Augmentation

Robotic tasks like grasping and pushing rely on consistent object geometry and frictional properties [75, 76]. We address this by applying object texture augmentation with preserved visual roughness and geometry. Following the mesh segmentation in Sec. 5.1, we segment the object mesh and render with altered material properties. Specifically, albedo A^* sets the base color, roughness R^* controls surface scattering, and metallic M^* defines the metallic effect. By adjusting only the albedo A^* while keeping roughness R^* and metallic M^* fixed, and reapplying Eq. 4, we achieve object texture augmentation with consistent visual roughness and geometry. Examples are shown in Fig. 7c.

5.3 Distractor Placement in Cluttered Environments

Previous methods typically place distractors via inpainting using text-driven generative models [17, 16, 4]. We take a different approach by leveraging the meshes of the scene and distractors for physically plausible placement in Blender [77]. As shown in Fig. 7d, we first align the surface normal with Blender’s default gravity axis (Z-axis). This requires the user to manually select a mesh face whose surface normal is parallel to the gravity direction using the Blender API. A random position within the bounding box of Λ (Eq. 8) is sampled, and the distractor mesh — assigned a pseudo-mass of 1kg at its geometric center — is dropped to simulate its motion under gravity. The final placement of the distractor is determined by its stable resting state following the gravity-based simulation. The full simulation process is available in the supplementary video.

6 Conclusion

We propose the first framework that applies physically-based lighting augmentation on real-world human demonstrations for robotic manipulation. By decomposing robotic scenes into geometric and material properties, we perform lighting augmentation on a single frame and propagate it across the entire demonstration using finetuned Stable Video Diffusion. We validate our framework through qualitative and quantitative visual quality evaluations, 720 real-world trials under six varied lighting conditions using a 7-DoF robot, and complementary ablation studies. We further showcase augmentations on three additional environmental factors enabled by our framework. This work marks an initial step toward integrating physical realism into visual augmentation, with the potential to assist future research on improving imitation learning generalization under environmental variation.

7 Limitations and Future work

Environment Lighting Approximation. Although we provide physically-based lighting augmentation by simulating light-material interactions, the absence of an environment map that perfectly reconstructs the currently observed lighting leads to reduced performance. One example is shown in Fig. 8, where under high-intensity red LED lighting (4600 lux), the plastic pear and plate exhibit strong reflections, differing from our augmentation. The discrepancy results from the side-mounted high-intensity LED producing strong directional lighting, while the approximated environment map failed to capture this and provides primarily diffuse illumination with a shifted color tone. This is partially due to the limited precision of the single-view-based environment map approximation (32×16 resolution). Capturing current lighting using graphical equipment [62] to generate accurate environment maps could mitigate this issue. Future work will focus on improving lighting approximation and deriving high-precision environment maps from single-view input for robotic scenes.

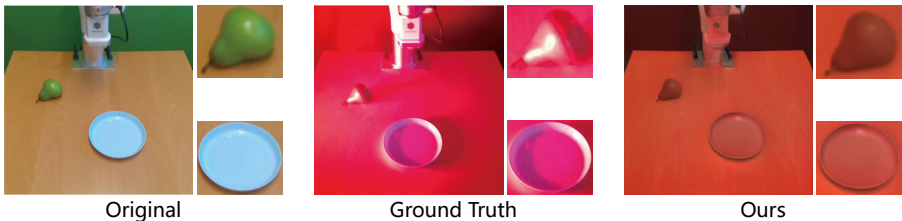


Figure 8: Failure cases observed under high-intensity lighting.

Efficiency. The current temporal propagation module only applies to lighting augmentation and does not extend to the other three environmental factors discussed in Sec. 5, as they are not captured by the curated SVD fine-tuning dataset. Consequently, augmentation for the additional factors is currently performed frame by frame, which makes the proposed applications more suitable for off-line augmentation of human demonstration data. Future work will focus on improving efficiency through selective optimization of geometric and material properties, taking into account environmental similarities in robotic data collection settings.

A Universal Lighting Composition. This paper focuses on using the proposed lighting augmentation framework to improve performance under currently observed lighting conditions, as the specific and quantified effects of different lighting on robot learning remain largely unknown. Future work will aim to systematically study how various lighting conditions impact policy performance and, based on this understanding, develop effective augmentation strategies for constructing a universal lighting composition to support lighting-invariant policies.

Visual-Physical Gap. The term *physically-based* in this paper refers to physically-based rendering. While we follow physically accurate light-material interactions from a computer graphics perspective, these effects are purely visual and do not affect motion dynamics, which is a critical aspect of robotic manipulation.

References

- [1] A. Mandlekar, D. Xu, J. Wong, S. Nasiriany, C. Wang, R. Kulkarni, L. Fei-Fei, S. Savarese, Y. Zhu, and R. Martín-Martín. What matters in learning from offline human demonstrations for robot manipulation. *arXiv preprint arXiv:2108.03298*, 2021.
- [2] S. Young, D. Gandhi, S. Tulsiani, A. Gupta, P. Abbeel, and L. Pinto. Visual imitation made easy. In J. Kober, F. Ramos, and C. Tomlin, editors, *Proceedings of the 2020 Conference on Robot Learning*, volume 155 of *Proceedings of Machine Learning Research*, pages 1992–2005. PMLR, 16–18 Nov 2021. URL <https://proceedings.mlr.press/v155/young21a.html>.
- [3] E. Jang, A. Irpan, M. Khansari, D. Kappler, F. Ebert, C. Lynch, S. Levine, and C. Finn. BC-z: Zero-shot task generalization with robotic imitation learning. In *5th Annual Conference on Robot Learning*, 2021. URL <https://openreview.net/forum?id=8kbp23tSGYv>.
- [4] Z. Mandi, H. Bharadhwaj, V. Moens, S. Song, A. Rajeswaran, and V. Kumar. Cacti: A 578 framework for scalable multi-task multi-scene visual imitation learning. *arxiv preprint 579. arXiv preprint arXiv:2212.05711*, 580, 2022.
- [5] A. Xie, L. Lee, T. Xiao, and C. Finn. Decomposing the generalization gap in imitation learning for visual robotic manipulation. In *2024 IEEE International Conference on Robotics and Automation (ICRA)*, pages 3153–3160. IEEE, 2024.
- [6] K. Burns, Z. Witzel, J. I. Hamid, T. Yu, C. Finn, and K. Hausman. What makes pre-trained visual representations successful for robust manipulation? *arXiv preprint arXiv:2312.12444*, 2023.
- [7] E. Xing, A. Gupta, S. Powers, and V. Dean. Kitchenshift: Evaluating zero-shot generalization of imitation-based policy learning under domain shifts. In *NeurIPS 2021 Workshop on Distribution Shifts: Connecting Methods and Applications*, 2021.
- [8] F. Lin, Y. Hu, P. Sheng, C. Wen, J. You, and Y. Gao. Data scaling laws in imitation learning for robotic manipulation. *arXiv preprint arXiv:2410.18647*, 2024.
- [9] S. Jin, R. Wang, M. Zahid, and F. T. Pokorny. How physics and background attributes impact video transformers in robotic manipulation: A case study on planar pushing. In *2024 IEEE/RSJ International Conference on Intelligent Robots and Systems (IROS)*, pages 7391–7398. IEEE, 2024.
- [10] W. Pumacay, I. Singh, J. Duan, R. Krishna, J. Thomason, and D. Fox. The colosseum: A benchmark for evaluating generalization for robotic manipulation. *arXiv preprint arXiv:2402.08191*, 2024.
- [11] J. Gao, A. Xie, T. Xiao, C. Finn, and D. Sadigh. Efficient data collection for robotic manipulation via compositional generalization. *arXiv preprint arXiv:2403.05110*, 2024.
- [12] R. Liu, A. Canberk, S. Song, and C. Vondrick. Differentiable robot rendering. *arXiv preprint arXiv:2410.13851*, 2024.
- [13] P. Vitiello, K. Dreczkowski, and E. Johns. One-shot imitation learning: A pose estimation perspective. *arXiv preprint arXiv:2310.12077*, 2023.
- [14] J. Tobin, R. Fong, A. Ray, J. Schneider, W. Zaremba, and P. Abbeel. Domain randomization for transferring deep neural networks from simulation to the real world. In *2017 IEEE/RSJ international conference on intelligent robots and systems (IROS)*, pages 23–30. IEEE, 2017.
- [15] S. James, P. Wohlhart, M. Kalakrishnan, D. Kalashnikov, A. Irpan, J. Ibarz, S. Levine, R. Hadsell, and K. Bousmalis. Sim-to-real via sim-to-sim: Data-efficient robotic grasping via randomized-to-canonical adaptation networks. In *Proceedings of the IEEE/CVF conference on computer vision and pattern recognition*, pages 12627–12637, 2019.

- [16] Z. Chen, S. Kiami, A. Gupta, and V. Kumar. Genau: Retargeting behaviors to unseen situations via generative augmentation. *arXiv preprint arXiv:2302.06671*, 2023.
- [17] T. Yu, T. Xiao, A. Stone, J. Tompson, A. Brohan, S. Wang, J. Singh, C. Tan, J. Peralta, B. Ichter, et al. Scaling robot learning with semantically imagined experience. *arXiv preprint arXiv:2302.11550*, 2023.
- [18] L. Wang, D. M. Tran, R. Cui, T. TG, M. Chandraker, and J. R. Frisvad. Materialist: Physically based editing using single-image inverse rendering. *arXiv preprint arXiv:2501.03717*, 2025.
- [19] A. Blattmann, T. Dockhorn, S. Kulal, D. Mendeleevitch, M. Kilian, D. Lorenz, Y. Levi, Z. English, V. Voleti, A. Letts, et al. Stable video diffusion: Scaling latent video diffusion models to large datasets. *arXiv preprint arXiv:2311.15127*, 2023.
- [20] S. Dasari, F. Ebert, S. Tian, S. Nair, B. Bucher, K. Schmeckpeper, S. Singh, S. Levine, and C. Finn. Robonet: Large-scale multi-robot learning. *arXiv preprint arXiv:1910.11215*, 2019.
- [21] M. Laskin, K. Lee, A. Stooke, L. Pinto, P. Abbeel, and A. Srinivas. Reinforcement learning with augmented data. *Advances in neural information processing systems*, 33:19884–19895, 2020.
- [22] I. Kostrikov, D. Yarats, and R. Fergus. Image augmentation is all you need: Regularizing deep reinforcement learning from pixels. *arXiv preprint arXiv:2004.13649*, 2020.
- [23] N. Hansen, R. Jangir, Y. Sun, G. Alenyà, P. Abbeel, A. A. Efros, L. Pinto, and X. Wang. Self-supervised policy adaptation during deployment. *arXiv preprint arXiv:2007.04309*, 2020.
- [24] B. Li, V. François-Lavet, T. Doan, and J. Pineau. Domain adversarial reinforcement learning. *arXiv preprint arXiv:2102.07097*, 2021.
- [25] H. Bharadhwaj, J. Vakil, M. Sharma, A. Gupta, S. Tulsiani, and V. Kumar. Roboagent: Generalization and efficiency in robot manipulation via semantic augmentations and action chunking. In *2024 IEEE International Conference on Robotics and Automation (ICRA)*, pages 4788–4795. IEEE, 2024.
- [26] L. Y. Chen, K. Hari, K. Dharmarajan, C. Xu, Q. Vuong, and K. Goldberg. Mirage: Cross-embodiment zero-shot policy transfer with cross-painting. *arXiv preprint arXiv:2402.19249*, 2024.
- [27] R. Rombach, A. Blattmann, D. Lorenz, P. Esser, and B. Ommer. High-resolution image synthesis with latent diffusion models. In *Proceedings of the IEEE/CVF conference on computer vision and pattern recognition*, pages 10684–10695, 2022.
- [28] L. Zhang, A. Rao, and M. Agrawala. Adding conditional control to text-to-image diffusion models. In *Proceedings of the IEEE/CVF International Conference on Computer Vision*, pages 3836–3847, 2023.
- [29] M. Minderer, A. Gritsenko, A. Stone, M. Neumann, D. Weissenborn, A. Dosovitskiy, A. Mahendran, A. Arnab, M. Dehghani, Z. Shen, et al. Simple open-vocabulary object detection. In *European Conference on Computer Vision*, pages 728–755. Springer, 2022.
- [30] S. Wang, C. Saharia, C. Montgomery, J. Pont-Tuset, S. Noy, S. Pellegrini, Y. Onoe, S. Laszlo, D. J. Fleet, R. Soricut, et al. Imagen editor and editbench: Advancing and evaluating text-guided image inpainting. In *Proceedings of the IEEE/CVF conference on computer vision and pattern recognition*, pages 18359–18369, 2023.
- [31] K. Sargent, Z. Li, T. Shah, C. Herrmann, H.-X. Yu, Y. Zhang, E. R. Chan, D. Lagun, L. Fei-Fei, D. Sun, et al. Zeronvs: Zero-shot 360-degree view synthesis from a single real image. *arXiv preprint arXiv:2310.17994*, 2023.

- [32] J. J. Yu, F. Forghani, K. G. Derpanis, and M. A. Brubaker. Long-term photometric consistent novel view synthesis with diffusion models. In *Proceedings of the IEEE/CVF International Conference on Computer Vision*, pages 7094–7104, 2023.
- [33] B. Mildenhall, P. P. Srinivasan, M. Tancik, J. T. Barron, R. Ramamoorthi, and R. Ng. Nerf: Representing scenes as neural radiance fields for view synthesis. *Communications of the ACM*, 65(1):99–106, 2021.
- [34] L. Y. Chen, C. Xu, K. Dharmarajan, M. Z. Irshad, R. Cheng, K. Keutzer, M. Tomizuka, Q. Vuong, and K. Goldberg. Rovi-aug: Robot and viewpoint augmentation for cross-embodiment robot learning. *arXiv preprint arXiv:2409.03403*, 2024.
- [35] X. Zhang, M. Chang, P. Kumar, and S. Gupta. Diffusion meets dagger: Supercharging eye-in-hand imitation learning. *arXiv preprint arXiv:2402.17768*, 2024.
- [36] A. Zhou, M. J. Kim, L. Wang, P. Florence, and C. Finn. Nerf in the palm of your hand: Corrective augmentation for robotics via novel-view synthesis. In *Proceedings of the IEEE/CVF Conference on Computer Vision and Pattern Recognition*, pages 17907–17917, 2023.
- [37] B. Van Hoorick, R. Wu, E. Ozguroglu, K. Sargent, R. Liu, P. Tokmakov, A. Dave, C. Zheng, and C. Vondrick. Generative camera dolly: Extreme monocular dynamic novel view synthesis. In *European Conference on Computer Vision*, pages 313–331. Springer, 2025.
- [38] A. Mandlekar, S. Nasiriany, B. Wen, I. Akinola, Y. Narang, L. Fan, Y. Zhu, and D. Fox. Mimicgen: A data generation system for scalable robot learning using human demonstrations. *arXiv preprint arXiv:2310.17596*, 2023.
- [39] Z. Jiang, Y. Xie, K. Lin, Z. Xu, W. Wan, A. Mandlekar, L. Fan, and Y. Zhu. Dexmimicgen: Automated data generation for bimanual dexterous manipulation via imitation learning. *arXiv preprint arXiv:2410.24185*, 2024.
- [40] C. Garrett, A. Mandlekar, B. Wen, and D. Fox. Skillmimicgen: Automated demonstration generation for efficient skill learning and deployment. *arXiv preprint arXiv:2410.18907*, 2024.
- [41] S. Nasiriany, A. Maddukuri, L. Zhang, A. Parikh, A. Lo, A. Joshi, A. Mandlekar, and Y. Zhu. Robocasa: Large-scale simulation of everyday tasks for generalist robots. *arXiv preprint arXiv:2406.02523*, 2024.
- [42] L. Yang, H. Suh, T. Zhao, B. P. Graesdal, T. Kelestemur, J. Wang, T. Pang, and R. Tedrake. Physics-driven data generation for contact-rich manipulation via trajectory optimization. *arXiv preprint arXiv:2502.20382*, 2025.
- [43] D. Azinovic, T.-M. Li, A. Kaplanyan, and M. Nießner. Inverse path tracing for joint material and lighting estimation. In *Proceedings of the IEEE/CVF conference on computer vision and pattern recognition*, pages 2447–2456, 2019.
- [44] D. Eigen and R. Fergus. Predicting depth, surface normals and semantic labels with a common multi-scale convolutional architecture. In *Proceedings of the IEEE international conference on computer vision*, pages 2650–2658, 2015.
- [45] C. Liu, K. Kim, J. Gu, Y. Furukawa, and J. Kautz. Planercnn: 3d plane detection and reconstruction from a single image. In *Proceedings of the IEEE/CVF Conference on Computer Vision and Pattern Recognition*, pages 4450–4459, 2019.
- [46] J. Zhu, F. Luan, Y. Huo, Z. Lin, Z. Zhong, D. Xi, R. Wang, H. Bao, J. Zheng, and R. Tang. Learning-based inverse rendering of complex indoor scenes with differentiable monte carlo raytracing. In *SIGGRAPH Asia 2022 Conference Papers*, pages 1–8, 2022.
- [47] S. Bell, K. Bala, and N. Snavely. Intrinsic images in the wild. *ACM Transactions on Graphics (TOG)*, 33(4):1–12, 2014.

- [48] Z. Li and N. Snavely. Cgintrinsics: Better intrinsic image decomposition through physically-based rendering. In *Proceedings of the European conference on computer vision (ECCV)*, pages 371–387, 2018.
- [49] S. Sengupta, J. Gu, K. Kim, G. Liu, D. W. Jacobs, and J. Kautz. Neural inverse rendering of an indoor scene from a single image. In *Proceedings of the IEEE/CVF International Conference on Computer Vision*, pages 8598–8607, 2019.
- [50] J. T. Barron and J. Malik. Intrinsic scene properties from a single rgb-d image. In *Proceedings of the IEEE Conference on Computer Vision and Pattern Recognition*, pages 17–24, 2013.
- [51] M.-A. Gardner, K. Sunkavalli, E. Yumer, X. Shen, E. Gambaretto, C. Gagné, and J.-F. Lalonde. Learning to predict indoor illumination from a single image. *arXiv preprint arXiv:1704.00090*, 2017.
- [52] M.-A. Gardner, Y. Hold-Geoffroy, K. Sunkavalli, C. Gagné, and J.-F. Lalonde. Deep parametric indoor lighting estimation. In *Proceedings of the IEEE/CVF International Conference on Computer Vision*, pages 7175–7183, 2019.
- [53] Z. Li, J. Shi, S. Bi, R. Zhu, K. Sunkavalli, M. Hašan, Z. Xu, R. Ramamoorthi, and M. Chandraker. Physically-based editing of indoor scene lighting from a single image. In *European Conference on Computer Vision*, pages 555–572. Springer, 2022.
- [54] Z. Li, K. Sunkavalli, and M. Chandraker. Materials for masses: Svbrdf acquisition with a single mobile phone image. In *Proceedings of the European conference on computer vision (ECCV)*, pages 72–87, 2018.
- [55] R. Zhu, Z. Li, J. Matai, F. Porikli, and M. Chandraker. Irisformer: Dense vision transformers for single-image inverse rendering in indoor scenes. In *Proceedings of the IEEE/CVF Conference on Computer Vision and Pattern Recognition*, pages 2822–2831, 2022.
- [56] Y. Yao, J. Zhang, J. Liu, Y. Qu, T. Fang, D. McKinnon, Y. Tsin, and L. Quan. Neilf: Neural incident light field for physically-based material estimation. In *European Conference on Computer Vision*, pages 700–716. Springer, 2022.
- [57] Z. Li, L. Wang, M. Cheng, C. Pan, and J. Yang. Multi-view inverse rendering for large-scale real-world indoor scenes. In *Proceedings of the IEEE/CVF Conference on Computer Vision and Pattern Recognition*, pages 12499–12509, 2023.
- [58] J. Bao, G. Chen, and S. Cui. Photometric inverse rendering: Shading cues modeling and surface reflectance regularization. *arXiv preprint arXiv:2408.06828*, 2024.
- [59] L. Lyu, A. Tewari, M. Habermann, S. Saito, M. Zollhöfer, T. Leimkühler, and C. Theobalt. Diffusion posterior illumination for ambiguity-aware inverse rendering. *ACM Transactions on Graphics (TOG)*, 42(6):1–14, 2023.
- [60] L. Wu, R. Zhu, M. B. Yaldiz, Y. Zhu, H. Cai, J. Matai, F. Porikli, T.-M. Li, M. Chandraker, and R. Ramamoorthi. Factorized inverse path tracing for efficient and accurate material-lighting estimation. In *Proceedings of International Conference on Computer Vision (ICCV)*, pages 3848–3858. IEEE, 2023.
- [61] J. J. Park, A. Holynski, and S. M. Seitz. Seeing the world in a bag of chips. In *Proceedings of Computer Vision and Pattern Recognition (CVPR)*, pages 1417–1427. IEEE, 2020.
- [62] P. Debevec. Rendering synthetic objects into real scenes: Bridging traditional and image-based graphics with global illumination and high dynamic range photography. In *Acm siggraph 2008 classes*, pages 1–10. 2008.
- [63] P. Debevec. A median cut algorithm for light probe sampling. In *ACM SIGGRAPH 2008 classes*, pages 1–3. 2008.

- [64] Poly Haven. Poly haven hdris, 2025. URL <https://polyhaven.com/hdris>. Accessed: 2025-03-19.
- [65] Ambientcg. URL <https://ambientcg.com/>. Accessed: March 4, 2025.
- [66] B. Burley and W. D. A. Studios. Physically-based shading at disney. In *Acm Siggraph*, volume 2012, pages 1–7. vol. 2012, 2012.
- [67] J. T. Kajiya. The rendering equation. In *Proceedings of the 13th annual conference on Computer graphics and interactive techniques*, pages 143–150, 1986.
- [68] L. Zhang, A. Rao, and M. Agrawala. Scaling in-the-wild training for diffusion-based illumination harmonization and editing by imposing consistent light transport. In *The Thirteenth International Conference on Learning Representations*.
- [69] R. Zhang, P. Isola, A. A. Efros, E. Shechtman, and O. Wang. The unreasonable effectiveness of deep features as a perceptual metric. In *Proceedings of the IEEE conference on computer vision and pattern recognition*, pages 586–595, 2018.
- [70] Z. Wang, A. C. Bovik, H. R. Sheikh, and E. P. Simoncelli. Image quality assessment: from error visibility to structural similarity. *IEEE transactions on image processing*, 13(4):600–612, 2004.
- [71] K. He, X. Zhang, S. Ren, and J. Sun. Deep residual learning for image recognition. In *Proceedings of the IEEE conference on computer vision and pattern recognition*, pages 770–778, 2016.
- [72] H. Walke, K. Black, A. Lee, M. J. Kim, M. Du, C. Zheng, T. Zhao, P. Hansen-Estruch, Q. Vuong, A. He, V. Myers, K. Fang, C. Finn, and S. Levine. Bridgedata v2: A dataset for robot learning at scale. In *Conference on Robot Learning (CoRL)*, 2023.
- [73] A. Kirillov, E. Mintun, N. Ravi, H. Mao, C. Rolland, L. Gustafson, T. Xiao, S. Whitehead, A. C. Berg, W.-Y. Lo, et al. Segment anything. In *Proceedings of the IEEE/CVF international conference on computer vision*, pages 4015–4026, 2023.
- [74] B. Calli, A. Walsman, A. Singh, S. Srinivasa, P. Abbeel, and A. M. Dollar. Benchmarking in manipulation research: The ycb object and model set and benchmarking protocols. *arXiv preprint arXiv:1502.03143*, 2015.
- [75] J. Mahler, F. T. Pokorny, B. Hou, M. Roderick, M. Laskey, M. Aubry, K. Kohlhoff, T. Kröger, J. Kuffner, and K. Goldberg. Dex-net 1.0: A cloud-based network of 3d objects for robust grasp planning using a multi-armed bandit model with correlated rewards. In *2016 IEEE international conference on robotics and automation (ICRA)*, pages 1957–1964. IEEE, 2016.
- [76] C. Chi, Z. Xu, S. Feng, E. Cousineau, Y. Du, B. Burchfiel, R. Tedrake, and S. Song. Diffusion policy: Visuomotor policy learning via action diffusion. *The International Journal of Robotics Research*, page 02783649241273668, 2023.
- [77] Blender Online Community. Blender - a 3d modelling and rendering package. <https://www.blender.org>, 2018.